Mortar multiscale methods for flow in porous media

Ivan Yotov
Department of Mathematics, University of Pittsburgh

OASCR Applied Mathematics PI Meeting
LLNL, May 22-24, 2007

Joint work with Todd Arbogast, Gergina Pencheva, and Mary F. Wheeler, The University of Texas at Austin

Outline

- Motivation
- A multiscale mortar mixed finite element method
- A priori error estimates
- A domain decomposition algorithm
- A posteriori error estimates
- Mortar and subdomain adaptivity
- A relationship between multiscale mortar MFE methods and subgrid upscaling methods
- Multiscale mortar for two-phase flow

Motivation: flow in heterogeneous porous media

Heterogeneous permeability varies on a fine scale.
Full fine scale grid resolution $\Rightarrow$ large, highly coupled system of equations $\Rightarrow$ solution is computationally intractable

- Variational Multiscale Method
  - Hughes et al; Brezzi
  - Mixed FEM: Arbogast et al

- Multiscale Finite Elements
  - Hou, Wu, Cai, Efendiev et al
  - Mixed FEM: Chen and Hou; Aarnes et al

New approach: based on domain decomposition and mortar finite elements

More flexible - easy to improve global accuracy by refining the local mortar grid where needed

Multiscale finite element/subgrid upscaling methods

$$L_\epsilon u = f \quad \Rightarrow \quad u \in V : \; a(u,v) = (f,v) \; \forall\, v \in V.$$

Multiscale approximation: H - coarse grid, $h \approx \epsilon$ - fine grid (subgrid)

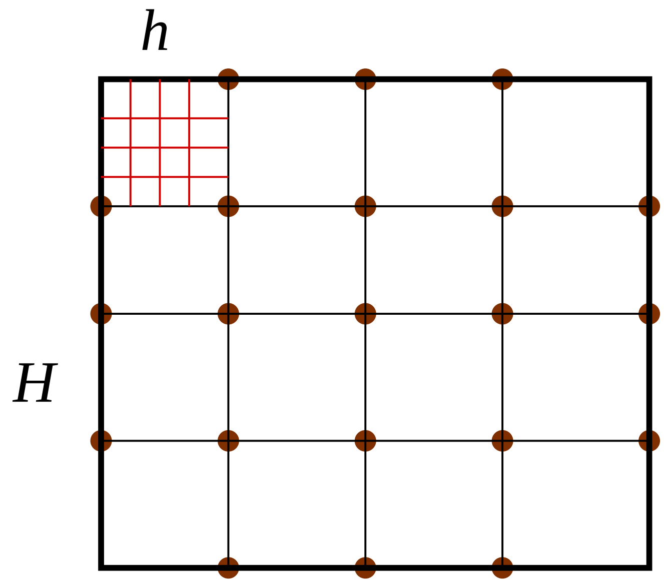

$$V_{H,h} = V_H + V_h'$$

Basis for $V_h'(E)$: $\phi_{h,i}^E$, $i = 1, \ldots, N_E$,

$$a_E(\phi_{H,i}^E + \phi_{h,i}^E, v_h) = 0 \quad \forall\, v_h \in V_h(E)$$

Multiscale solution: $u_{H,h} \in V_{H,h}$,

$$a(u_{H,h}, v_{H,h}) = (f, v_{H,h}) \quad \forall\, v_{H,h} \in V_{H,h}$$

Multiblock formulation for single phase flow

$\bar{\Omega} = \cup_{i=1}^{n} \bar{\Omega}_i$; $\Gamma_{ij} = \partial\Omega_i \cap \partial\Omega_j$

On each block Ω_i:

$$\mathbf{u} = -K\nabla p \quad \text{in } \Omega_i$$

$$\nabla \cdot \mathbf{u} = q \quad \text{in } \Omega_i$$

$$\mathbf{u} \cdot \nu = 0 \quad \text{on } \partial\Omega_i \cap \partial\Omega$$

On each interface Γ_{ij}:

$$p_i = p_j \quad \text{on } \Gamma_{ij}$$

$$[\mathbf{u} \cdot \nu]_{ij} = 0 \quad \text{on } \Gamma_{ij}$$

where

$$p_i = p|_{\partial\Omega_i}$$

$$[\mathbf{u} \cdot \nu]_{ij} \equiv \mathbf{u}|_{\Omega_i} \cdot \nu - \mathbf{u}|_{\Omega_j} \cdot \nu$$

Multiblock discretization spaces

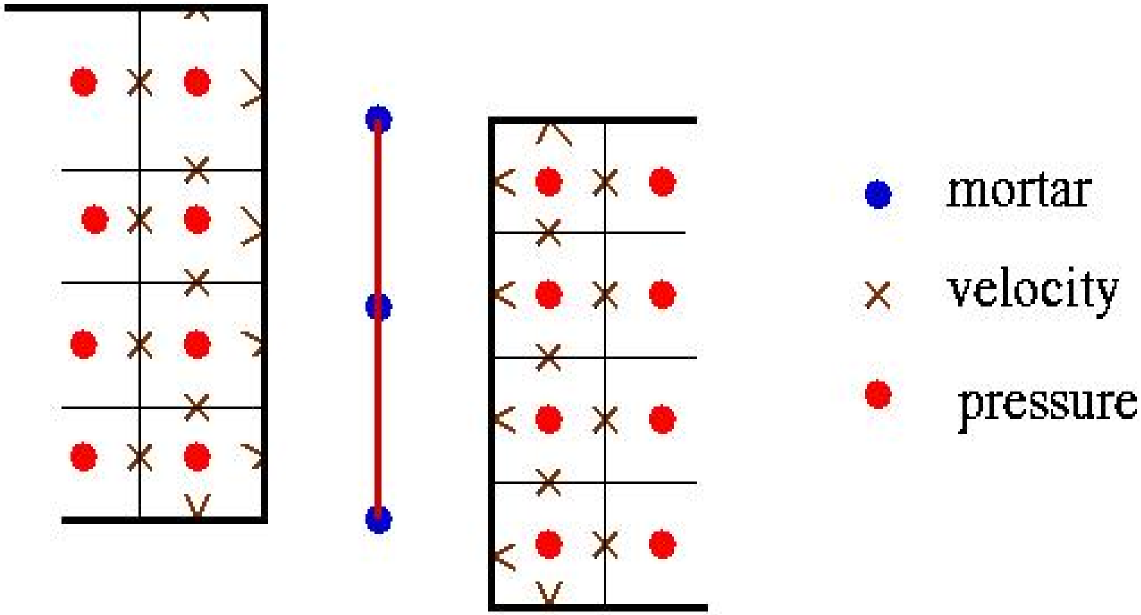

$$\mathbf{V}_h = \bigoplus_{i=1}^{n} \mathbf{V}_{h,i}, \quad W_h = \bigoplus_{i=1}^{n} W_{h,i}, \quad M_h = \bigoplus_{0 \le i < j \le n} M_{h,ij}$$

$$\lambda_h|_{\Gamma_{ij}} \in M_{h,ij}, \quad \int_{\Gamma_{ij}} [\mathbf{u}_h \cdot \nu]_{ij} \mu = 0, \mu \in M_{h,ij}.$$

Subdomain grids do not need to match.

The mortar mixed finite element method

Find $\mathbf{u}_h \in \mathbf{V}_h$, $p_h \in W_h$, $\lambda_h \in M_h$ s.t. for $1 \le i \le n$

$$(K^{-1}\mathbf{u}_h, \mathbf{v})_{\Omega_i} - (p_h, \nabla \cdot \mathbf{v})_{\Omega_i} + \langle \lambda_h, \mathbf{v} \cdot \nu_i \rangle_{\Gamma_i} = 0, \quad \mathbf{v} \in \mathbf{V}_{h,i},$$

$$(\nabla \cdot \mathbf{u}_h, w)_{\Omega_i} = (q, w)_{\Omega_i}, \quad w \in W_{h,i},$$

$$\sum_{i=1}^{n} \langle \mathbf{u}_h \cdot \nu_i, \mu \rangle_{\Gamma_i} = 0, \quad \mu \in M_h.$$

Stability, optimal convergence, superconvergence:
Y.(1996,97), Arbogast, Cowsar, Wheeler, Y. (2000)

Two-scale formulation: mortar upscaling

Two-scale problem:

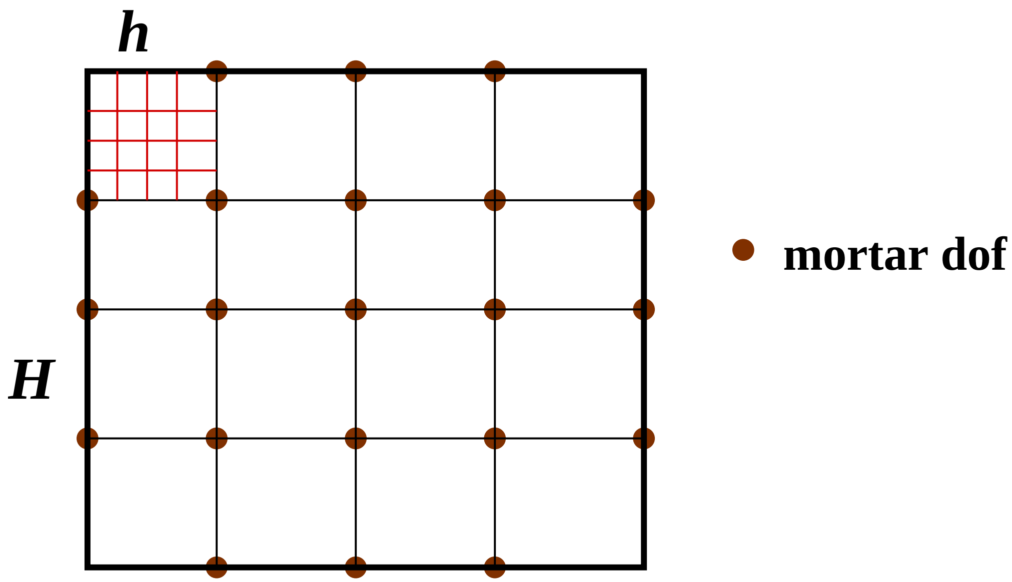

- Each block is an element of the coarse grid.
- Each block is discretized on the fine scale.
- A coarse mortar space on each interface.
- Result: Effective solution, fine scale on subdomains, coarse scale flux matching

Multiscale mortar mixed finite element method

Allow for different scales and polynomial approximations on interfaces and subdomains.

Assume

$$P_k \subset V_{h,i}, \quad P_l \subset W_{h,i}, \quad P_m \subset M_H, \; m \geq k+1$$

Find $\mathbf{u}_h \in \mathbf{V}_h$, $p_h \in W_h$, $\lambda_H \in M_H$ s.t. for $1 \leq i \leq n$

$$(K^{-1}\mathbf{u}_h, \mathbf{v})_{\Omega_i} - (p_h, \nabla \cdot \mathbf{v})_{\Omega_i} + \langle \lambda_H, \mathbf{v} \cdot \nu_i \rangle_{\Gamma_i} = 0, \quad \mathbf{v} \in \mathbf{V}_{h,i},$$

$$(\nabla \cdot \mathbf{u}_h, w)_{\Omega_i} = (q, w)_{\Omega_i}, \quad w \in W_{h,i},$$

$$\sum_{i=1}^{n} \langle \mathbf{u}_h \cdot \nu_i, \mu \rangle_{\Gamma_i} = 0, \quad \mu \in M_H.$$

Stability assumption:

$$\|\mu\|_{0,\Gamma_{i,j}} \leq C(\|\mathcal{Q}_{h,i}\mu\|_{0,\Gamma_{i,j}} + \|\mathcal{Q}_{h,j}\mu\|_{0,\Gamma_{i,j}}), \quad \mu \in M_H, \; 1 \leq i < j \leq n.$$

An approximation result

Weakly continuous velocities:

$$\mathbf{V}_{h,0} = \left\{ \mathbf{v} \in \mathbf{V}_h : \sum_{i=1}^{n} \langle \mathbf{v}|_{\Omega_i} \cdot \nu_i, \mu \rangle_{\Gamma_i} = 0 \ \ \forall \ \ \mu \in M_H \right\}.$$

Equivalent formulation: find $\mathbf{u}_h \in \mathbf{V}_{h,0}$ and $p_h \in W_h$ such that

$$(K^{-1}\mathbf{u}_h, \mathbf{v}) - (p_h, \nabla \cdot \mathbf{v}) = 0, \quad \mathbf{v} \in \mathbf{V}_{h,0},$$

$$(\nabla \cdot \mathbf{u}_h, w) = (q, w), \quad w \in W_h$$

Interpolation operator $\Pi_0 : \mathbf{V} \to \mathbf{V}_{h,0}$ such that

$$(\nabla \cdot (\Pi_0 \mathbf{q} - \mathbf{q}), w)_\Omega = 0, \quad w \in W_h.$$

$$\|\Pi_0 \mathbf{q} - \mathbf{q}\|_0 \le C \sum_{i=1}^{n} \left(\|\mathbf{q}\|_{r,\Omega_i} h^r + \|\mathbf{q}\|_{r+1/2,\Omega_i} h^r H^{1/2} \right), \quad 1 \le r \le k+1$$

A priori error estimates

Theorem:

$$\|\mathbf{u}-\mathbf{u}_h\| \le C(H^{m+1/2}+h^{k+1}), \quad \|\nabla\cdot(\mathbf{u}-\mathbf{u}_h)\| \le Ch^{l+1}$$

$$|||\mathbf{u}-\mathbf{u}_h||| \le C(H^{m+1/2}+h^{k+1}H^{1/2})$$

$$\|p-p_h\| \le C(H^{m+3/2}+h^{k+1}H+h^{l+1})$$

$$|||p-p_h||| \le CH\|\mathbf{u}-\mathbf{u}_h\|_{H(div)}$$

Balance $\|\mathbf{u}-\mathbf{u}_h\|$ or $|||p-p_h|||$ error terms (with $l=k$):

$$H = h^{\frac{k+1}{m+1/2}} \Rightarrow \|\mathbf{u}-\mathbf{u}_h\| \le Ch^{k+1}, \quad |||p-p_h||| \le Ch^{k+1+\frac{k+1}{m+1/2}}$$

For example, RT_0, $k=0$, and quadratic mortars, $m=2$,

$$H = h^{2/5} : \|\mathbf{u}-\mathbf{u}_h\| \le Ch, \quad \|p-p_h\| \le Ch, \quad |||p-p_h||| \le Ch^{1+2/5}$$

Parallel domain decomposition

Glowinski and Wheeler (1988), Y. (1996)

Two types of subdomain problems:

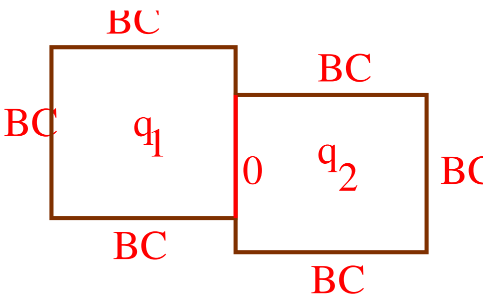

$$g_H(\mu) = \sum_{i=1}^{n} \langle \bar{\mathbf{u}}_{h,i} \cdot \nu_i, \mu \rangle_{\Gamma_i}$$

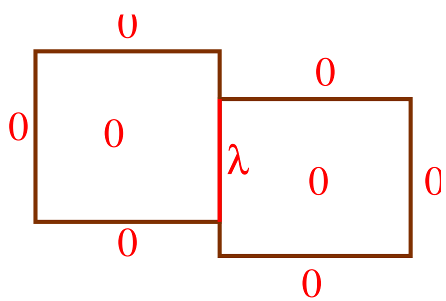

$$\begin{aligned} a_{H,i}(\lambda, \mu) &= -\langle \mathbf{u}^*_{h,i}(\lambda) \cdot \nu_i, \mu \rangle_{\Gamma_i} \\ a_H(\lambda, \mu) &= \sum_{i=1}^{n} a_{H,i}(\lambda, \mu) \end{aligned}$$

The solution $(\mathbf{u}_h, p_h, \lambda_H)$ to the original problem satisfies

$$A_H \lambda_H = g_H \quad \text{or} \quad a_H(\lambda_H, \mu) = g(\mu), \quad \forall \mu \in M_H,$$

$$\text{with } \mathbf{u}_h = \mathbf{u}^*_h(\lambda_H) + \bar{\mathbf{u}}_h, \quad p_h = p^*_h(\lambda_H) + \bar{p}_h.$$

Interface iteration

Lemma The interface operator $A_H : M_H \to M_H$ is symmetric and positive semi-definite.

$$a_{H,i}(\lambda, \mu) = (K^{-1}\mathbf{u}^*_{h,i}(\lambda), \mathbf{u}^*_{h,i}(\mu)).$$

$A_H : \lambda_H \to [\mathbf{u}^*_h(\lambda_H) \cdot \nu]$ is a Steklov-Poincare operator.

Apply the Conjugate Gradient method for $A_H \lambda_H = g_H$.

Computing the action of the operator (needed at each CG iteration):

- Given mortar data $\lambda_H \in \mathcal{M}_H$, project onto subdomain grids:

$$\lambda_H \to Q_{h_i}\lambda_H$$

- Solve local problems in parallel with boundary data $Q_{h_i}\lambda_H$
- Project fluxes onto the mortar space and compute the jump:

$$\mathbf{u}_{h,i} \cdot \nu_i \to Q^T_{h_i}\mathbf{u}_{h,i} \cdot \nu_i, \quad A_H\lambda_H = Q^T_{h_1}\mathbf{u}_{h,1} \cdot \nu_1 + Q^T_{h_2}\mathbf{u}_{h,2} \cdot \nu_2$$

Balancing preconditioner

Bourgat, Glowinski, Le Tallec, and Vidrascu (1989),
Mandel and Brezina (1996), Cowsar, Mandel, and Wheeler (1995),
Pencheva and Y (2003)

$$A_H = \sum A_{H,i}$$

$$M_H^{-1} = \left(\sum A_{H,i}^{-1} \right) A_{H,0}^{-1}$$

Condition number estimate:

Theorem

$$\mathrm{cond}(B_{bal}^{-1} A_H) \leq C(1 + \log(\tilde{H}/h))^2,$$

where C does not depend on h, H, and jumps in K.

Numerical experiments

m	H	$\|\|p - p_h\|\|$	$\|\|\mathbf{u} - \mathbf{u}_h\|\|$	$\|\|\|p - p_h\|\|\|$	$\|\|\|\mathbf{u} - \mathbf{u}_h\|\|\|$	$\|\|\|p - \lambda_H\|\|\|$	
						full K	*diag K*
2	$h^{1/2}$	1	1	1.5	1.25	1.25	1.5
1	$2h$	1	1	2	1.5	1.5	2

Table 1: Theoretical convergence rates for quadratic and linear mortars.

Example 1:

$$p(x,y) = x^3y^4 + x^2 + \sin(xy)\cos(y), \quad K = \begin{pmatrix} (x+1)^2 + y^2 & \sin(xy) \\ \sin(xy) & (x+1)^2 \end{pmatrix}.$$

Example 2:

$$p(x,y) = \begin{cases} x^2y^3 + \cos(xy) \\ \left(\frac{2x+9}{20}\right)^2 y^3 + \cos\left(\frac{2x+9}{20}y\right) \end{cases}, \quad K = \begin{cases} I, & 0 \le x \le 1/2, \\ 10 * I, & 1/2 \le x \le 1 \end{cases}$$

Computed solution for Example 1

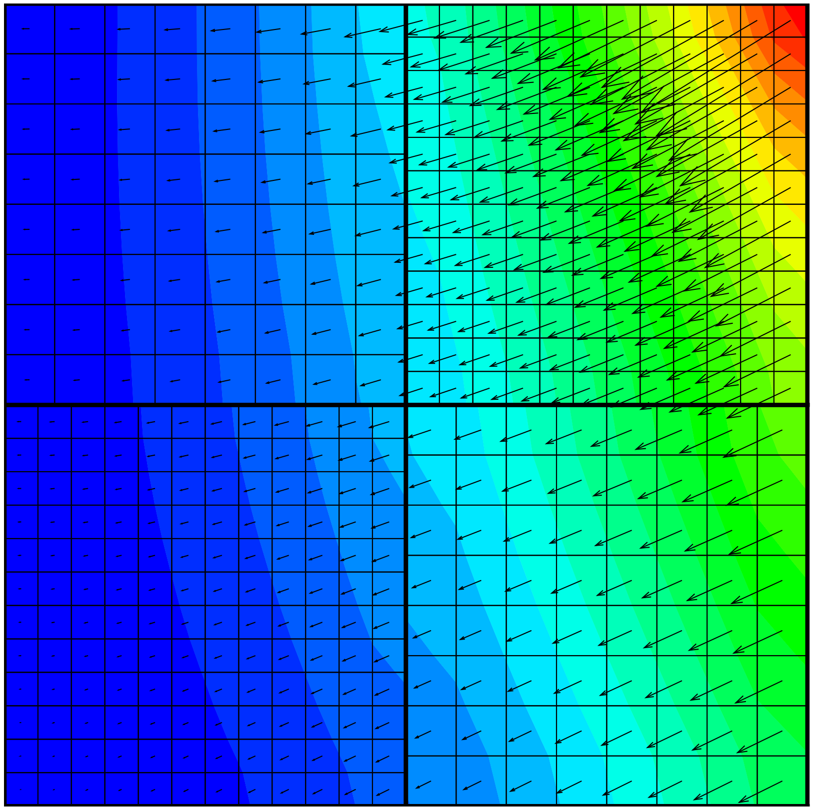

A. *Discontinuous quadratic mortars*

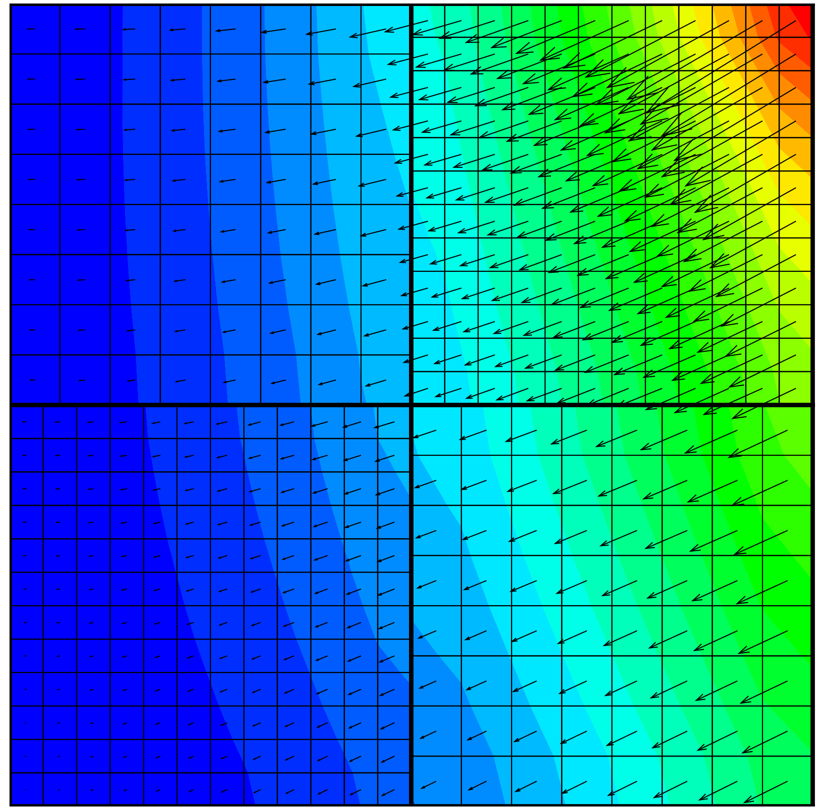

B. *Discontinuous linear mortars*

Computed pressure (shade) and velocity (arrows).

Convergence rates for Example 1

$1/h$	*iter.*	$\|\|p-p_h\|\|$	$\|\|\mathbf{u}-\mathbf{u}_h\|\|$	$\|\|\|p-p_h\|\|\|$	$\|\|\|\mathbf{u}-\mathbf{u}_h\|\|\|$	$\|\|\|p-\lambda_H\|\|\|$
4	8	2.64E-1	2.03E-1	4.62E-2	2.13E-2	4.45E-2
16	13	6.37E-2	4.86E-2	2.83E-3	1.81E-3	2.72E-3
64	15	1.59E-2	1.21E-2	1.75E-4	1.60E-4	1.69E-4
256	16	3.98E-3	3.03E-3	1.09E-5	1.77E-5	1.08E-5
rate		$\mathcal{O}(h^{1.01})$	$\mathcal{O}(h^{1.01})$	$\mathcal{O}(h^{2.01})$	$\mathcal{O}(h^{1.71})$	$\mathcal{O}(h^{2.00})$

Continuous quadratic mortars on non-matching grids

$1/h$	*iter.*	$\|\|p-p_h\|\|$	$\|\|\mathbf{u}-\mathbf{u}_h\|\|$	$\|\|\|p-p_h\|\|\|$	$\|\|\|\mathbf{u}-\mathbf{u}_h\|\|\|$	$\|\|\|p-\lambda_H\|\|\|$
4	4	2.63E-1	2.04E-1	4.54E-2	2.35E-2	4.55E-2
8	7	1.28E-1	9.82E-2	1.14E-2	7.32E-3	1.13E-2
16	13	6.37E-2	4.86E-2	2.82E-3	2.23E-3	2.83E-3
32	18	3.18E-2	2.43E-2	7.01E-4	6.95E-4	7.05E-4
64	23	1.59E-2	1.21E-2	1.75E-4	2.24E-4	1.76E-4
128	23	7.95E-3	6.06E-3	4.36E-5	7.47E-5	4.40E-5
256	24	3.98E-3	3.03E-3	1.09E-5	2.54E-5	1.09E-5
rate		$\mathcal{O}(h^{1.01})$	$\mathcal{O}(h^{1.01})$	$\mathcal{O}(h^{2.00})$	$\mathcal{O}(h^{1.65})$	$\mathcal{O}(h^{2.00})$

Continuous linear mortars on non-matching grids

Error in the computed solution for Example 1

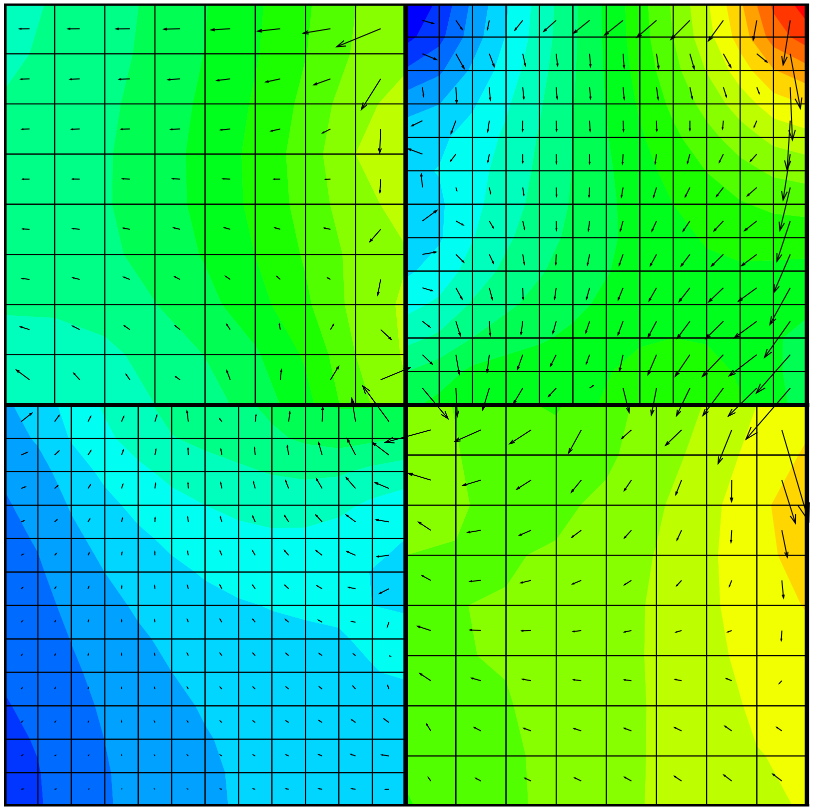

A. *Discontinuous quadratic mortars*

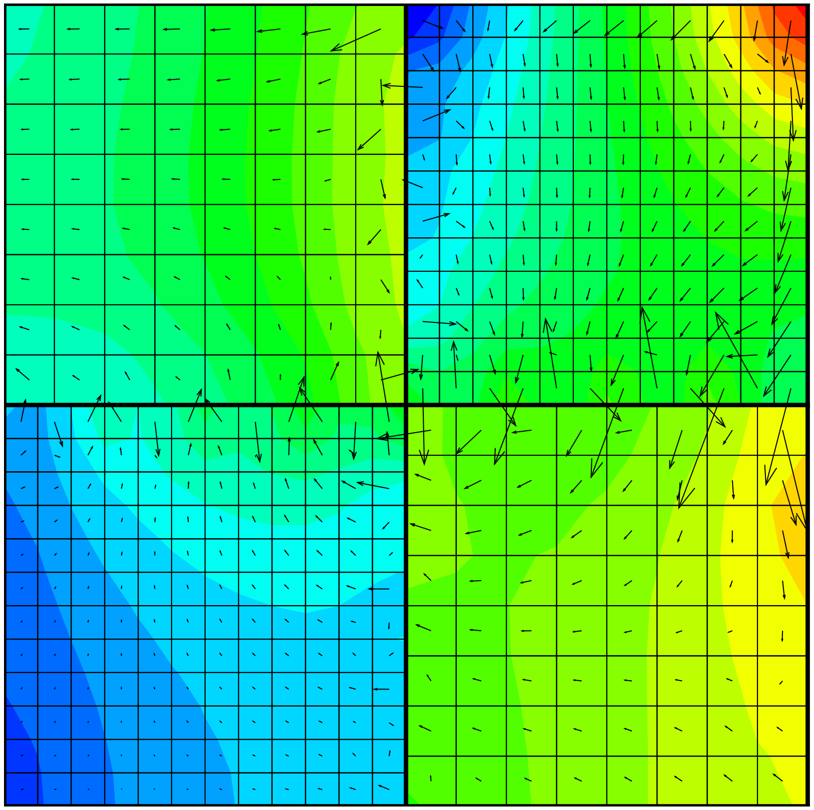

B. *Discontinuous linear mortars*

Error in computed pressure (shade) and velocity (arrows).

Iterative convergence for Example 2

$1/h$	*BalCG*		*CG*	
	cond.	*iter.*	*cond.*	*iter.*
4	1.83E+0	5	1.45E+1	8
16	2.49E+1	13	4.29E+1	20
64	2.33E+1	14	1.27E+2	29
256	2.96E+1	15	3.63E+2	45

Continuous quadratic mortars on matching grids

$1/h$	*BalCG*		*CG*	
	cond.	*iter.*	*cond.*	*iter.*
4	1.79E+1	5	3.91E+1	8
8	1.78E+1	8	3.74E+1	11
16	2.50E+1	13	3.82E+1	19
32	3.68E+1	19	6.60E+1	26
64	4.71E+1	23	1.30E+2	34
128	5.96E+1	24	2.58E+2	51
256	7.29E+1	24	5.16E+2	72

Continuous linear mortars on matching grids

A posteriori error estimates

- Estimate the error by computable quantities
- Use the error estimator to dynamically adapt the grids

$$E \in \mathcal{T}_h: \quad \omega_E^2 = \|K^{-1}\mathbf{u}_h + \nabla p_h\|_E^2 h_E^2 + \|f - \nabla \cdot \mathbf{u}_h\|_E^2 h_E^2 + \|\lambda_H - p_h\|_{\partial E \cap \Gamma}^2 h_E,$$

$$\tau \in \mathcal{T}^{\Gamma,H}: \quad \omega_\tau^2 = \|[\mathbf{u}_h \cdot \nu]\|_\tau^2 H_\tau^3,$$

$$\tilde{\omega}_E^2 = h_E^{-2}\omega_E^2, \quad \tilde{\omega}_\tau^2 = H_\tau^{-2}\omega_\tau^2.$$

Theorem (Upper bounds):

$$\|p - p_h\|^2 \le C \left\{ \sum_{E \in \mathcal{T}_h} \omega_E^2 + \sum_{\tau \in \mathcal{T}^{\Gamma,h}} \omega_\tau^2 \right\},$$

$$\|\mathbf{u} - \mathbf{u}_h\|_{H(\mathrm{div})}^2 \le C \left\{ \sum_{E \in \mathcal{T}_h} \tilde{\omega}_E^2 + \sum_{\tau \in \mathcal{T}^{\Gamma,h}} \tilde{\omega}_\tau^2 \right\}.$$

Residual-based estimates: lower bounds

Theorem:

$$\sum_{E\in\mathcal{T}_h} \omega_E^2 \quad + \quad \sum_{\tau\in\mathcal{T}^{\Gamma,H}} \omega_\tau^2 \leq C \Bigg(\|p-p_h\|^2 + \sum_{E\in\mathcal{T}_h} h_E^2 \|\mathbf{u}-\mathbf{u}_h\|^2_{H(\mathrm{div};E)}$$

$$+ \sum_{\tau\in\mathcal{T}^{\Gamma,H}} H_\tau \|\lambda-\lambda_H\|_\tau^2 + \sum_{\tau\in\mathcal{T}^{\Gamma,H}} h_{E,\tau}^{-1} H_\tau^3 \|\mathbf{u}-\mathbf{u}_h\|^2_{H(\mathrm{div};E_\tau)} \Bigg)$$

$$\sum_{E\in\mathcal{T}_h} \tilde{\omega}_E^2 + \sum_{\tau\in\mathcal{T}^{\Gamma,H}} \tilde{\omega}_\tau^2 \leq C \left(\sum_{E\in\mathcal{T}_h} h_E^{-2} \|p-p_h\|_E^2 + \|\mathbf{u}-\mathbf{u}_h\|^2_{H(\mathrm{div})} \right).$$

Efficient (lower) and reliable (upper) estimate for $p-p_h$:

$$C_1 \left(\sum_{E\in\mathcal{T}_h} \omega_E^2 + \sum_{\tau\in\mathcal{T}^{\Gamma,h}} \omega_\tau^2 \right) \leq \|p-p_h\|^2 \leq C_2 \left(\sum_{E\in\mathcal{T}_h} \omega_E^2 + \sum_{\tau\in\mathcal{T}^{\Gamma,H}} \omega_\tau^2 \right).$$

Adaptive mesh refinement algorithm

1. Solve the problem on a coarse (both subdomain and mortar) grid.

2. For each subdomain Ω_i

   (a) Compute

   $$\omega_i = \left(\sum_{E \in \mathcal{T}_{h,i}} \omega_E^2 + \sum_{\tau \in \mathcal{T}^{\Gamma_i,h}} \omega_\tau^2 \right)^{1/2}$$

   (b) If $\omega_i > .5 \max_{1 \le j \le n} \omega_j$, refine $\mathcal{T}_{h,i}$.

3. For each interface $\Gamma_{i,j}$, if either Ω_i or Ω_j has been refined m times, refine $\mathcal{T}_{h,i,j}$.

4. Solve the problem on the refined grid. If either the desired error tolerance or the maximum refinement level has been reached, exit; otherwise go to step 2.

Numerical experiments

Example 3: 2D problem with a boundary layer

$$p(x,y) = 1000\, x\, y\, e^{-10(x^2+y^2)}, \quad K = I$$

Dirichlet BCs; Continuous quadratic mortars

Example 4: 2D problem with highly oscilating tensor

$$K = \begin{cases} (105 - 100\sin(20\pi x)\sin(20\pi y)) * I, & 0 \le x, y \le 1/2 \text{ or} \\ & 1/2 \le x, y \le 1 \\ (105 - 100\sin(2\pi x)\sin(2\pi y)) * I, & \text{otherwise} \end{cases}$$

BCs: $p|_{x=0} = 1$, $p|_{x=1} = 0$, no flow on the rest of the boundary
Discontinuous quadratic mortars

Multiblock decomposition: 6×6 subdomains

Coarse grid: 2×2 on each subdomain and adaptive mesh refinement

Computed solution for Example 3

Pressure on the fourth grid level

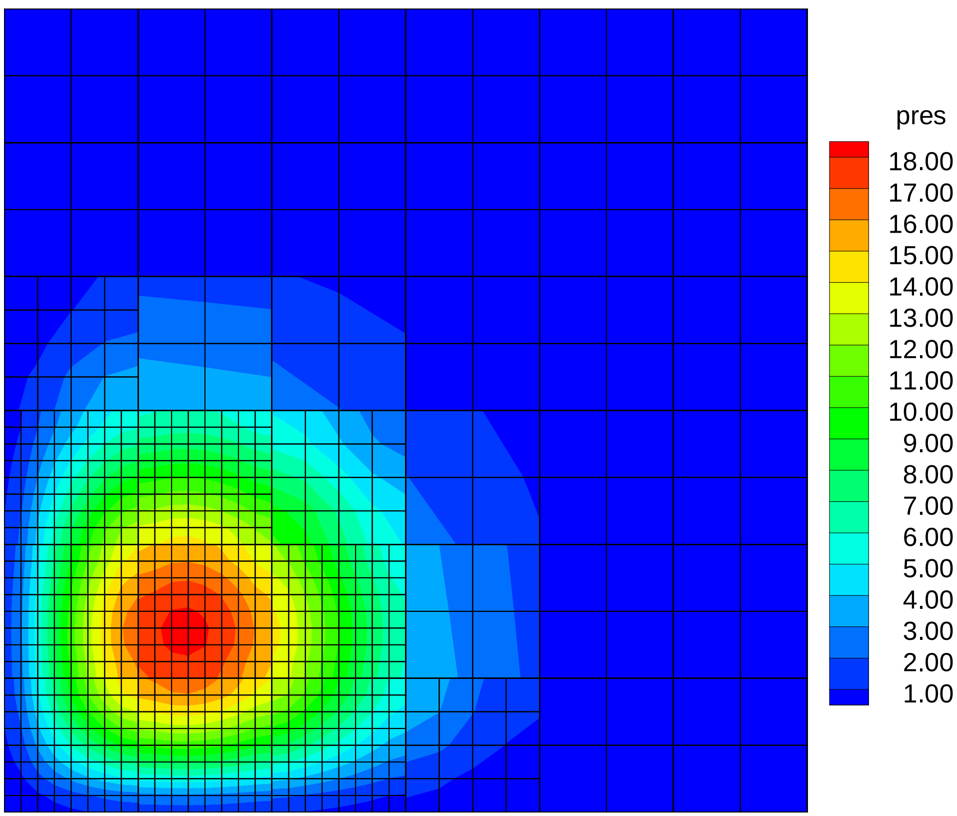

Discontinuous quadratic mortars

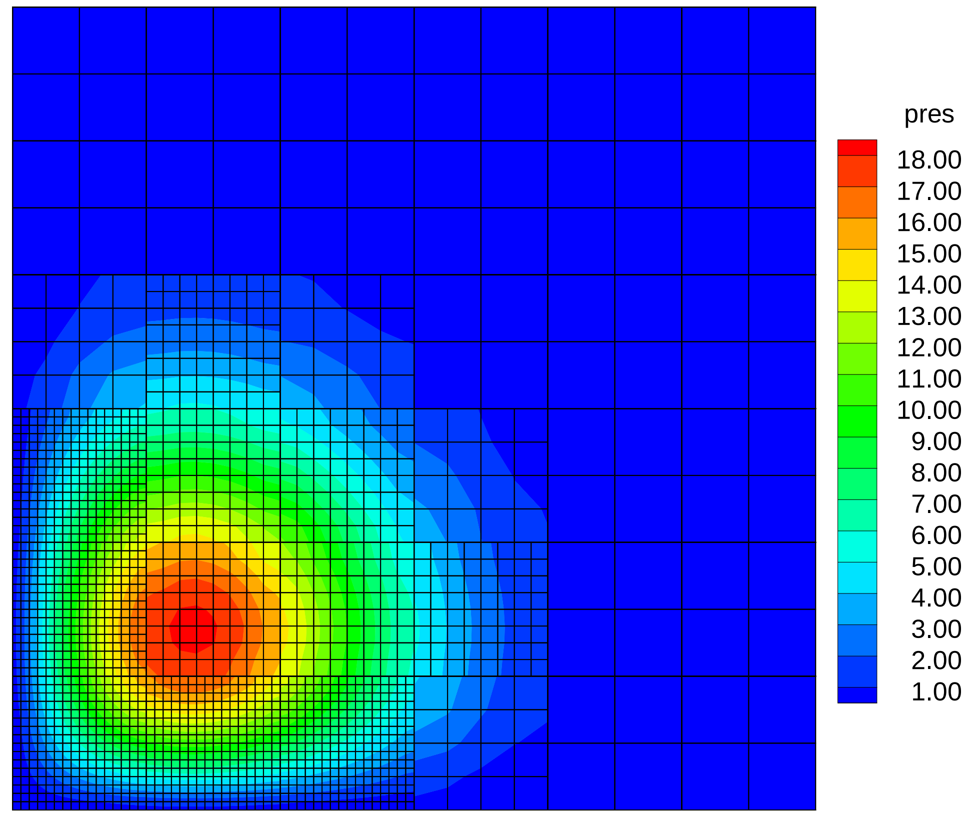

Discontinuous linear mortars

Computed solution for Example 4

Magnitude of the velocity on the fifth grid level

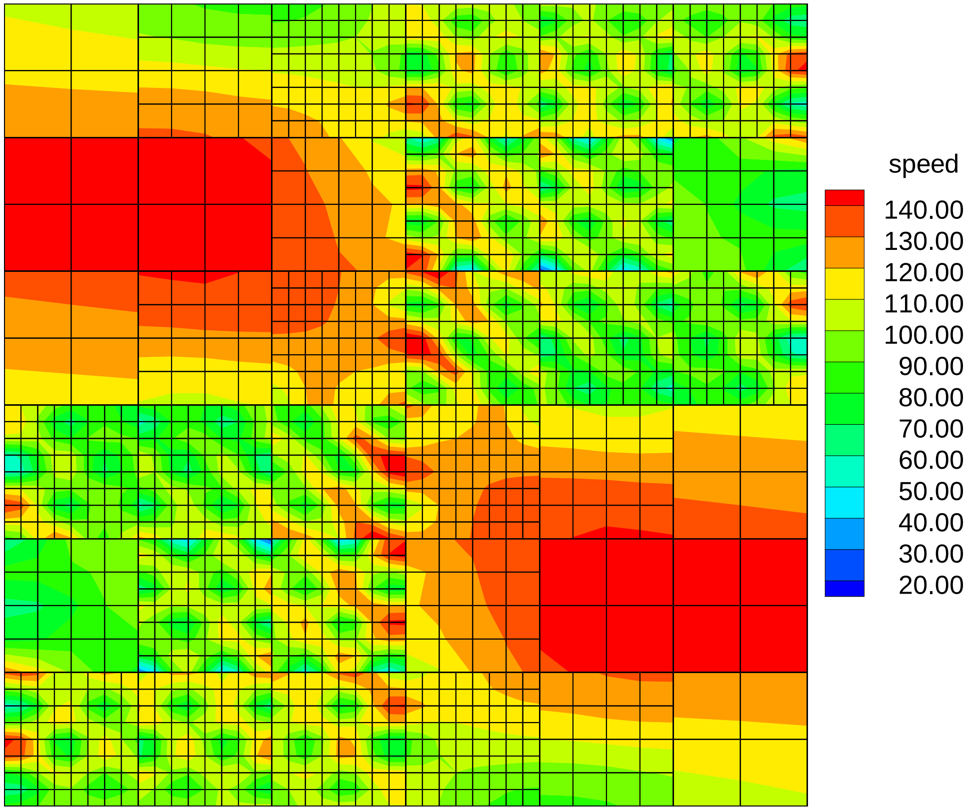

Discontinuous quadratic mortars

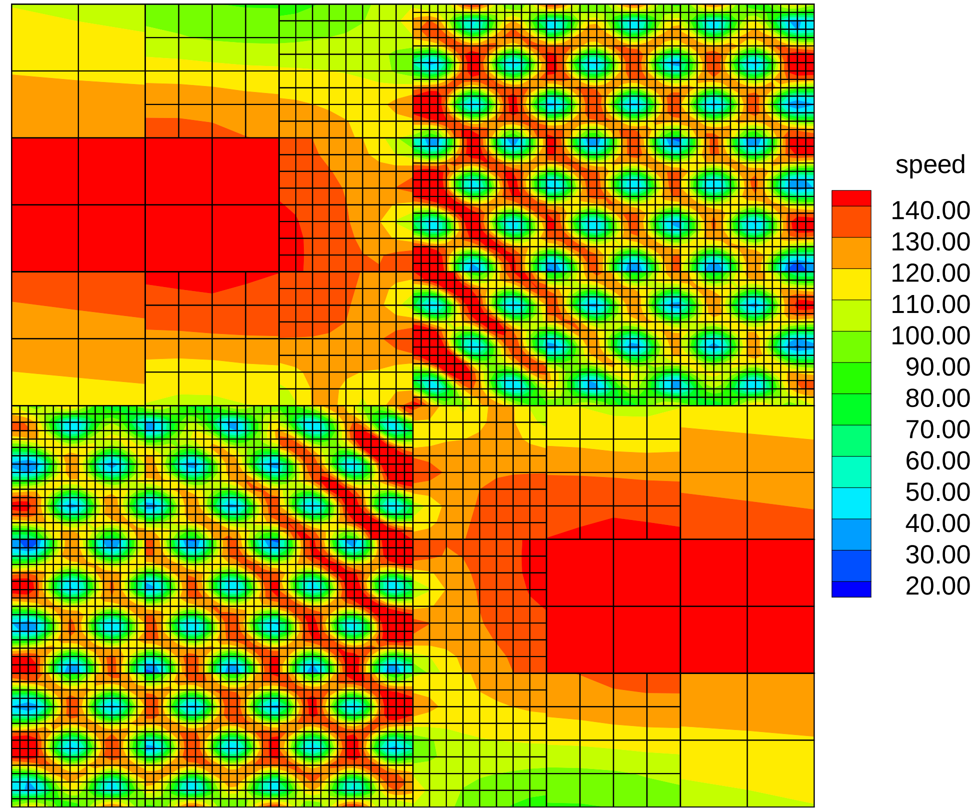

Discontinuous linear mortars

Relation to subgrid upscaling methods

Subgrid upscaling (Arbogast et. al.):

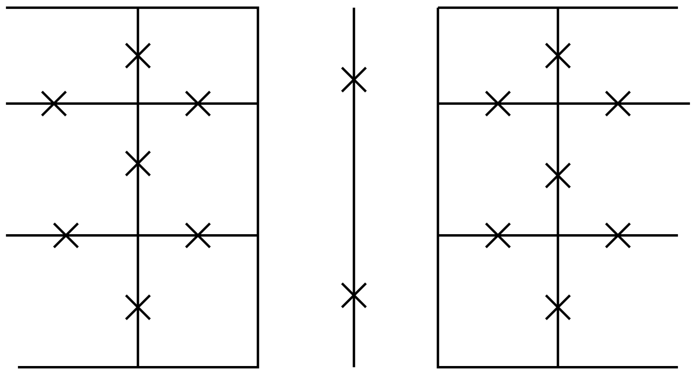

$\mathbf{V}_{h,1}^0 \qquad \mathbf{V}_H \qquad \mathbf{V}_{h,2}^0$

$$\mathbf{V}_h = \mathbf{V}_{h,1}^0 + \mathbf{V}_{h,2}^0 + \mathbf{V}_H$$

Multiscale mortar MFE:

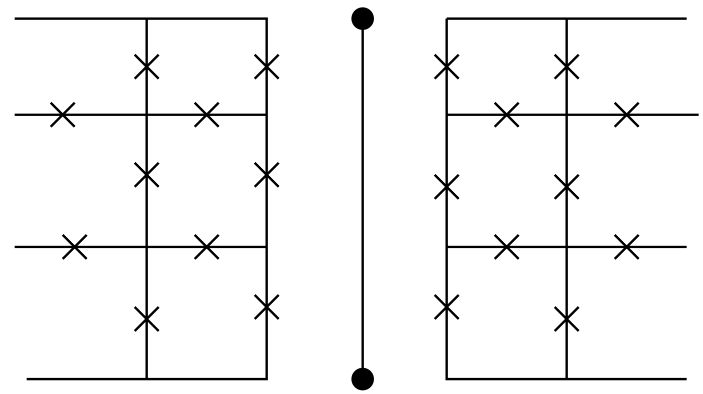

$\mathbf{V}_{h,1} \qquad M_H \qquad \mathbf{V}_{h,2}$

$$\mathbf{V}_{h,0} = \mathbf{V}_{h,1} + \mathbf{V}_{h,2} : \langle [\mathbf{v} \cdot \nu], \mu \rangle = 0, \mu \in M_H$$

Multiscale mortar MFE: fine scale velocity approximation on each coarse edge; coarse scale non-conforming error.

The two methods are related to the two (dual) non-overlapping domain decomposition formulations of Glowinski and Wheeler.

No boundary layer effect in the the multiscale mortar MFE method.

Note on the implementation

It is possible to solve

$$A_H \lambda_H = g_H$$

by solving for the discrete Green's functions

$$\mathbf{u}_h^*(\mu_H^j) \text{ for each mortar basis function } \mu_H^j \in M_H$$

and forming A_H explicitly.

In this case cost is comparable to subgrid upscaling and multiscale FEM.

The iterative approach is more efficient as long as the number of inerface iterations is less than the number of mortar degrees of freedom per subdomain.

Extension to two-phase flow

On each subdomain Ω_i:

$$\mathbf{U}_\alpha = -\frac{k_\alpha(S_\alpha)K}{\mu_\alpha}\rho_\alpha(\nabla P_\alpha - \rho_\alpha g \nabla D) \quad \text{(Darcy's law)}$$

$$\frac{\partial(\phi\rho_\alpha S_\alpha)}{\partial t} + \nabla\cdot\mathbf{U}_\alpha = q_\alpha \quad \text{(conservation of mass)}$$

On each interface Γ_{ij}:

$$P_\alpha|_{\Omega_i} = P_\alpha|_{\Omega_j}, \qquad [\mathbf{U}_\alpha\cdot\nu]_{ij} = 0.$$

On each Ω_i and Γ_{ij}:

$$S_w + S_n = 1, \qquad p_c(S_w) = P_n - P_w.$$

Domain decomposition

Interface operator $B_H : M_H \to M_H$

For $\lambda = (P_n^M, P_w^M) \in M_H$

$$B_H(\lambda) = ([\mathbf{U}_n^M(\lambda)], [\mathbf{U}_w^M(\lambda)]),$$

where $\mathbf{U}_\alpha^M(\lambda)$ is the mortar projection of the solution $\mathbf{U}_\alpha(\lambda) \cdot \nu$ to subdomain problems with Dirichlet boundary data λ.

The original problem is equivalent to solving for $\lambda \in M_H$ such that

$$B_H(\lambda) = 0.$$

IPARS implementation (CSM, UT Austin)

- Massively parallel - good speedup on 1000 nodes
- Multiblock - non-matching grids with mortars
- Multiphysics
  - single phase and two phase
  - black oil
  - compositional
  - geomechanics
- Multinumerics
  - cell-centered finite differences
  - multipoint flux mixed finite element methods
  - discontinuous Galerkin methods
- Advanced solvers
  - domain decomposition
  - Newton-Krylov solvers
  - physics-based preconditioners
  - algebraic multigrid

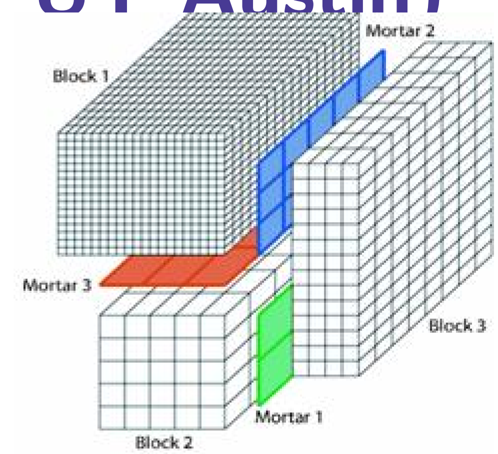

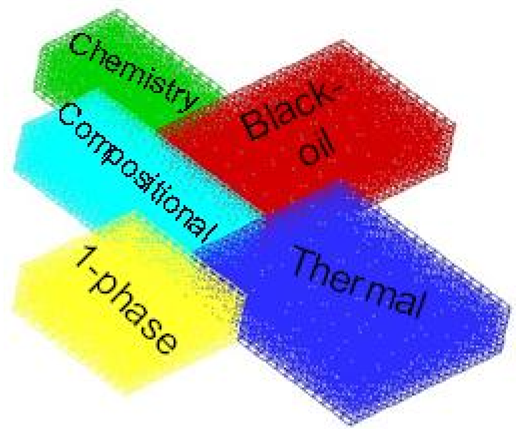

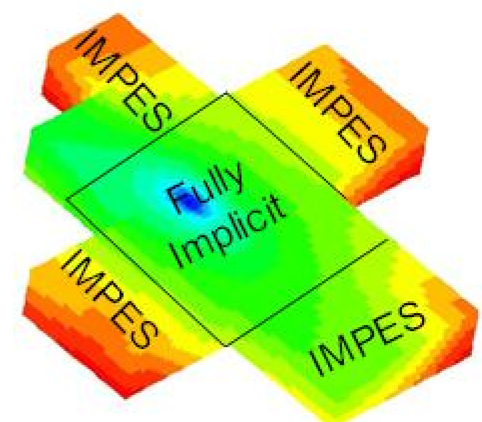

Scalability study in IPARS

SPE10 field
$85 \times 220 \times 60 = 1,122,000$ elements
1 injector, 4 producers

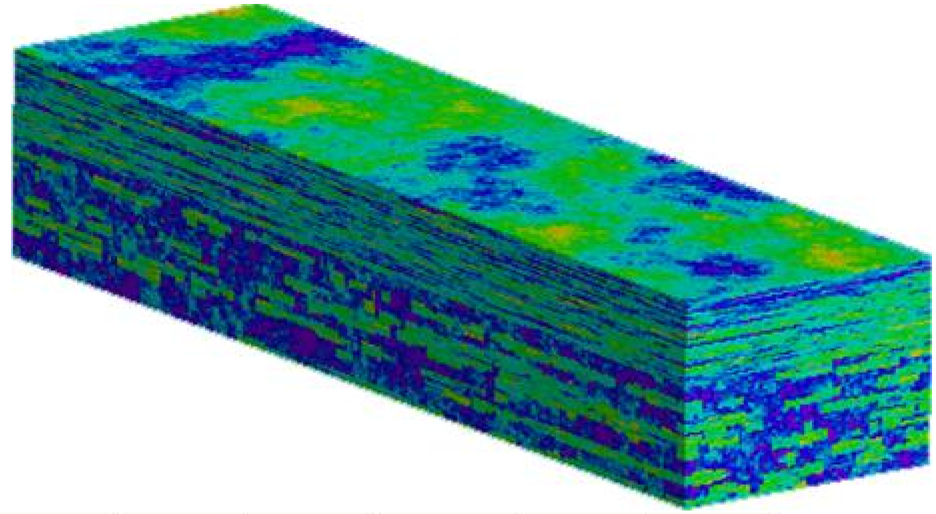

Num. Procs	10	20	30	50	80	100	150	200	256
Run Time (hr)	68.67	35.61	23.35	13.51	10.17	7.33	4.93	4.21	4.06

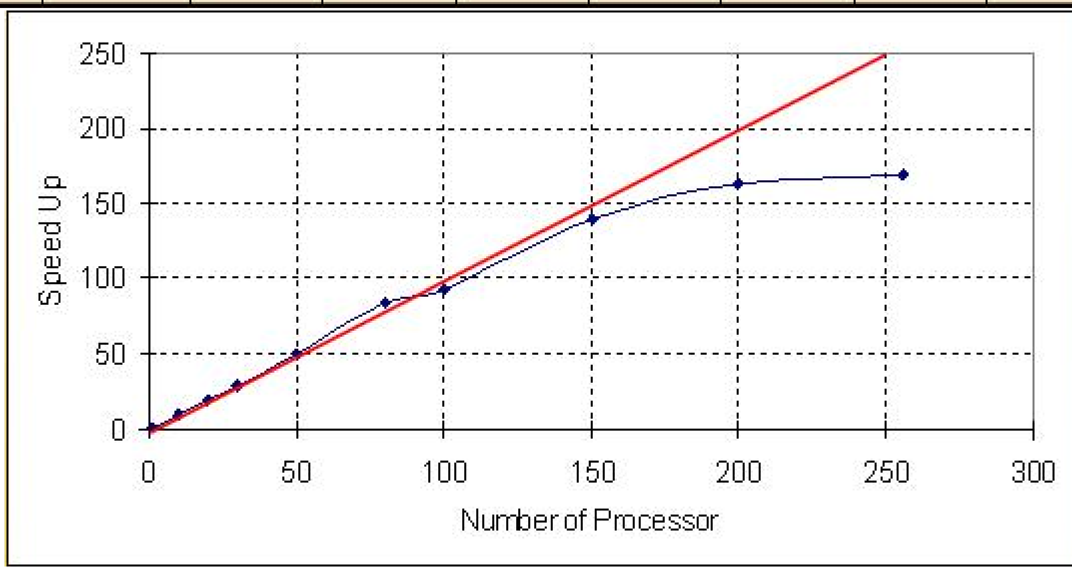

Multiscale computational experiment

SPE Comparative Solution Upscaling Project; Oil-water displacement in a horizontal cross-section 1200×2200 [ft]

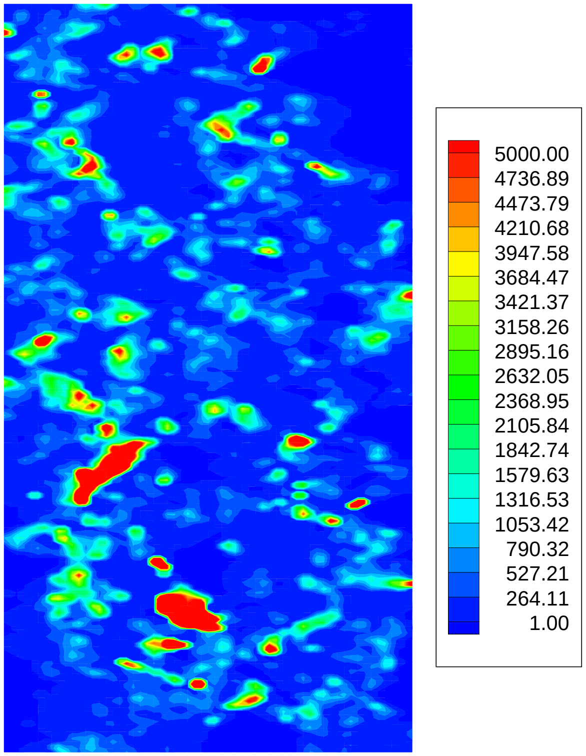

Permeability:
$2 * 10^{-3} - 2 * 10^{5}$

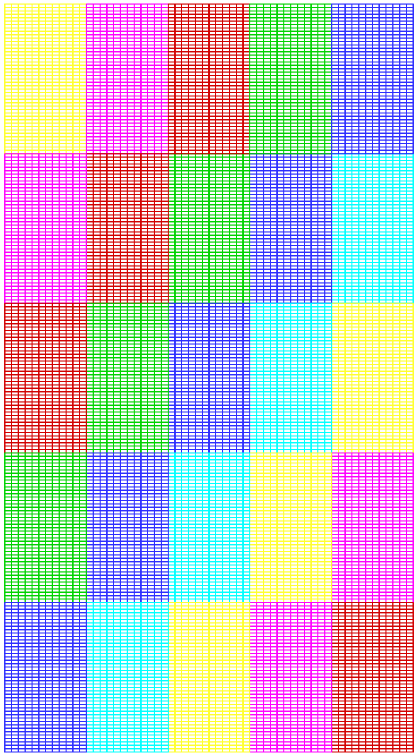

Computational grid 60×220
25 blocks: 5×5

Computed oil pressure profiles at 2951 days

Three runs: fine grid (1 block), multiblock run with a single linear mortar element on each interface (upscaled), multiblock run with refined mortars (6 elements) near the wells (adapted mortar).

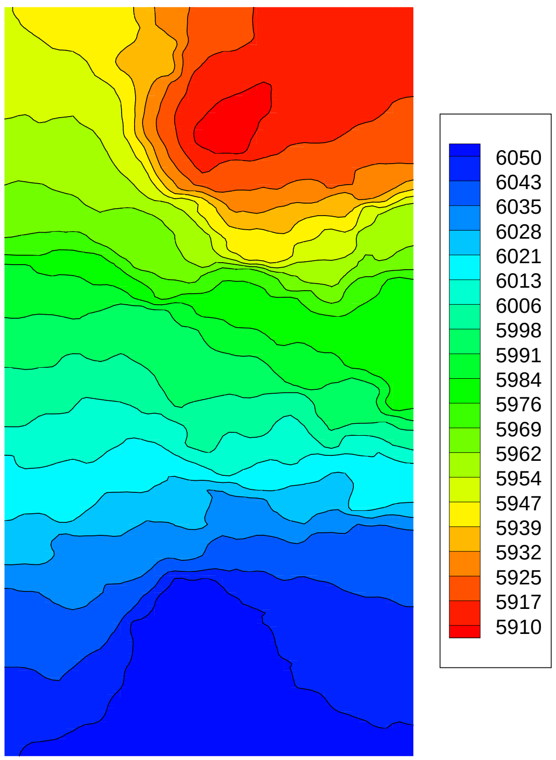

Fine grid solution

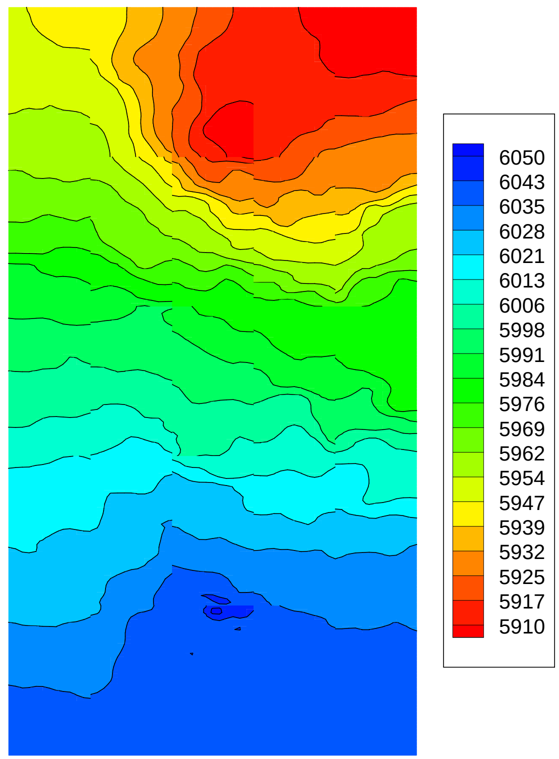

Upscaled solution

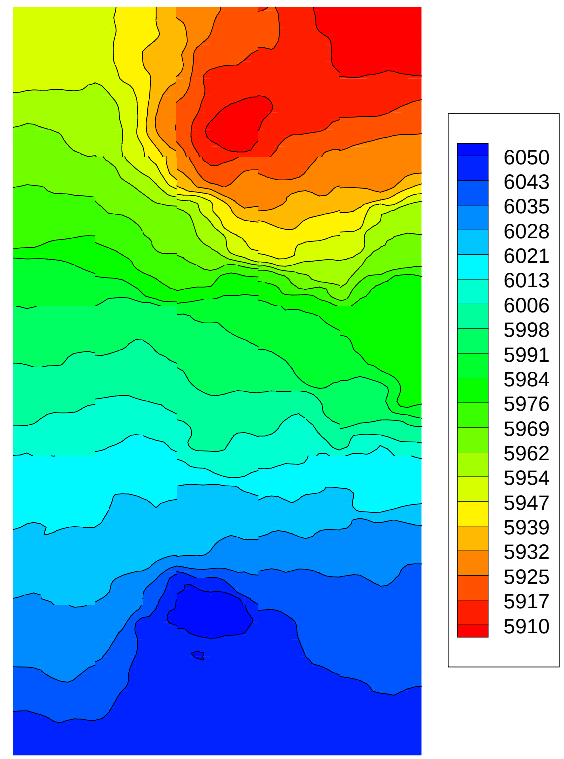

Adapted mortar solution

Computed oil concentration profiles at 2951 days

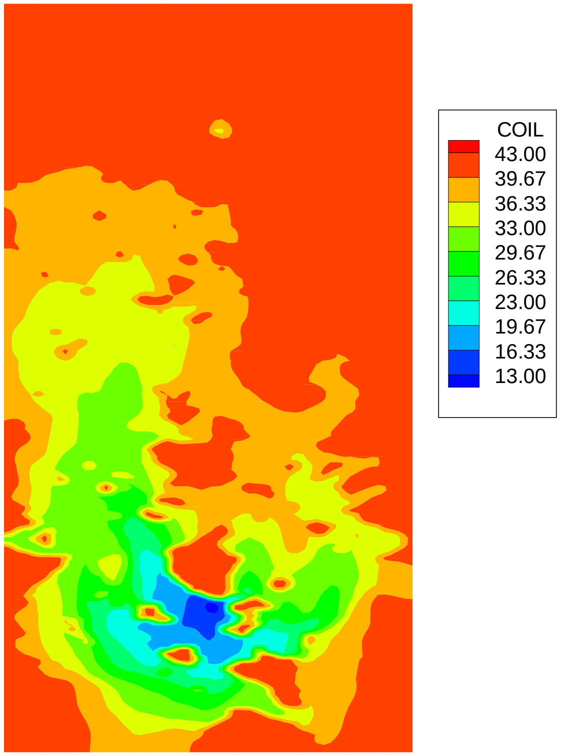

Fine grid solution

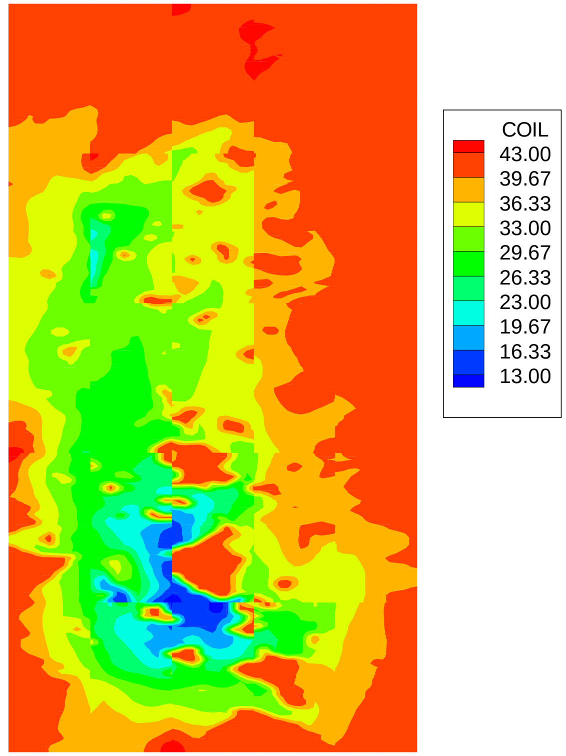

Upscaled solution

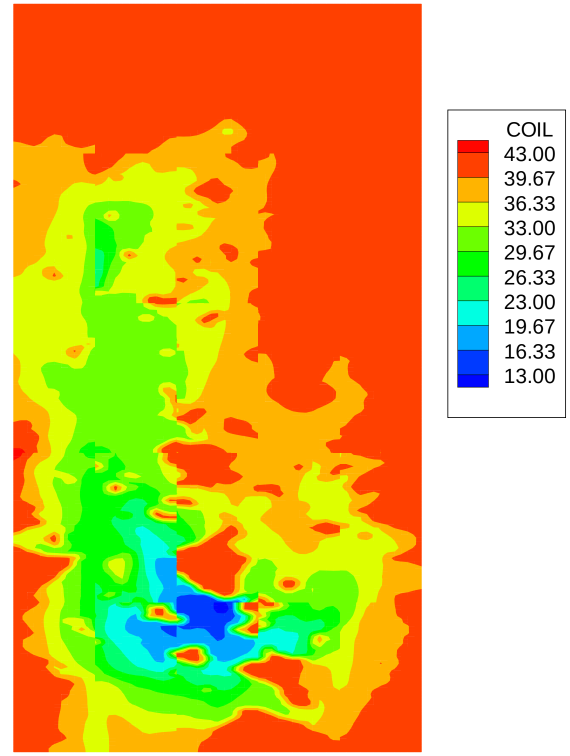

Adapted mortar solution

Adapted mortar increases production well rates accuracy by a factor of 2 at the cost of increasing CPU time by 50%.

Comparison of linear and quadratic mortars for two-phase flow

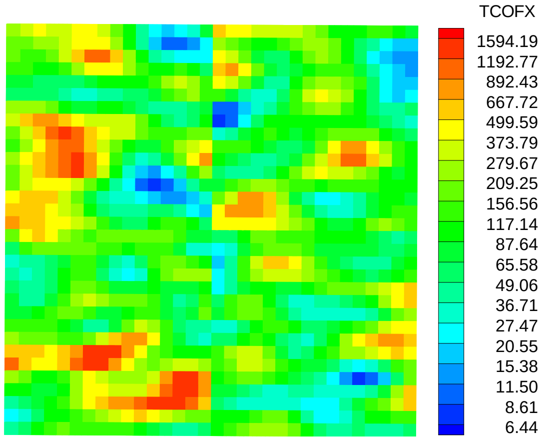

A. *Permeability field*

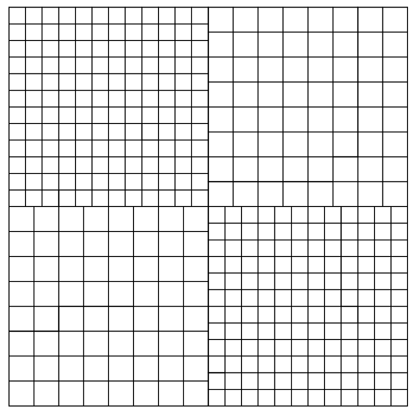

B. *Grids on the coarsest level*

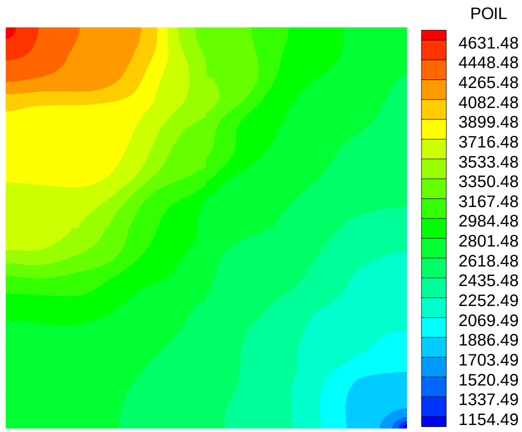

A. *Oil pressure*

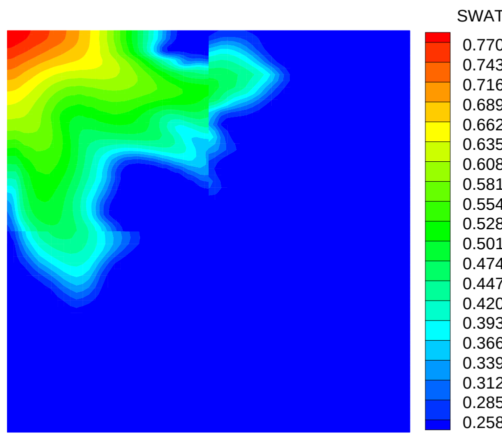

B. *Water saturation*

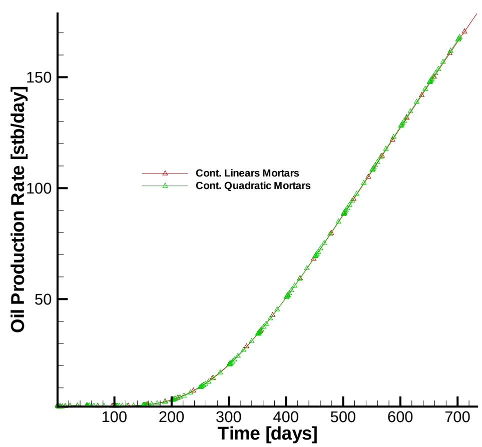

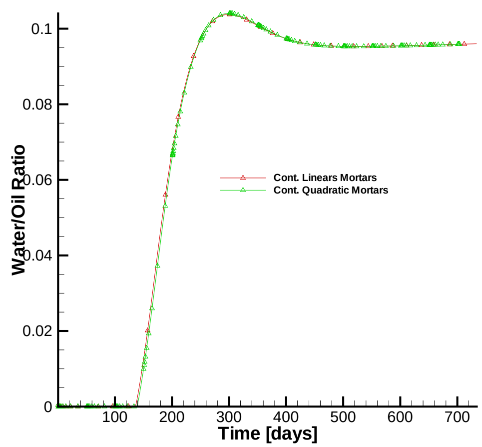

linear mortars		quadratic mortars	
mortar	GMRES	mortar	GMRES
4	51.2	2	42.3
8	72.7	3	54.4
16	92.6	4	63.9
32	155.2	6	75.9

Comparison of recovery curves.

Summary

- Mortar methods are related to multiscale methods
- Generalization of subgrid upscaling methods.
- Different scales and polynomial degrees on interfaces and subdomains.
- Effective solution: fine subdomain resolution with coarse-grid flux matching
- Optimal fine scale convergence
- Coarser mortars of higher degree are more computationally efficient than finer mortars of lower degree
- Extensions to multiphase flow in porous media
- Extensions to multiscale mortar DG-DG and DG-MFE methods

Current and future work

- Incorporate permeability modeling error in the error estimation
- Extensions to multiphysics problems
- Stochastic multiscale methods